Classification of Inherited Retinal Conditions with Machine Learning and Bio- Inspired Algorithms

[1]Suneetha K., [2]Rohaila Naaz, [3]Shish Dubey, [4]Govind Singh Panwar

Abstract*:* Over the past several years, a wide variety of ophthalmological disorders have seen an increase in the number of applications of machine learning. Inherited retinal disorders (IRC) are uncommon genetic conditions that present a distinct phenotype on fundus autofluorescence (FAF) imaging. Using machine learning with Bio- inspired algorithms; our goal was to develop a system that could automatically categorize distinct IRCs based on the appearance of FAF images. FAF imaging was used to conduct a retrospective study on patients who had presented to the Ophthalmology Department at the University of Paris Est Creteil between April 2007 and April 2019. Image preprocessing with Z-score normalization and Gabor Filter Bank (GFB) were utilized in order to glean characteristics from the images. The categorization was completed with the help of an innovative method called Chaotic Vortex Search Optimized Naive Bayes (CVSONB). Regarding the classifiers for inherited retinal diseases, performance metrics such as accuracy, f1 measure, sensitivity, and specificity were utilized. In this study, hereditary retinal disorders in FAF were automatically detected and classified utilizing an algorithm based on deep learning. The algorithm was developed as part of this investigation. As a result, the classifiers that were constructed demonstrated very promising outcomes. This model has the potential to become a diagnostic tool with more research and improvement, and it could also provide useful information for upcoming therapy approaches.

Keywords: inherited retinal conditions (IRC), fundus autofluorescence (FAF), Chaotic Vortex Search Optimized Naive Bayes (CVSONB), Z-score normalization, Gabor Filter Bank (GFB)

1. Introduction

A sizable, clinically and genetically diverse cluster of disorders known as inherited retinal diseases (IRDs) affects 1 in 3000 individuals globally and affects more than 2 million people. IRDs have a significant impact on both individuals and society since they are the most common hereditary types of human vision impairment [1]. In this situation, the development of noninvasive imaging tools has made it possible to measure IRDs more accurately. The diagnosis and monitoring of IRDs now rely heavily on images taken with a fundus camera in color auto fluorescence (FAF), and optical coherence tomography with great spatial resolution. One of the non-invasive FAF is a method for in vivo imaging methods for both of their metabolic maps' normal and retinal pathological fluorophores [2]. Early stages of retinal disease can be detected by FAF, in addition to phenotyping (because to

the changed intensities of FAF images). A topographical map of the spread of lipofuscin is produced thanks to the FAF's broad spectrum of wavelengths (500-800 nm) [3]. A2E, a byproduct of the ocular cycle, is N-retinyledene-N-retinylethanolamine, produces lipofuscin as a byproduct. It is particularly significant that FAF offered an accumulating lipofuscin mapping inside reticular pigment epithelium (RPE). Lipofuscin builds up in the RPE as a result of the RPE's ineffective phagocytosis of photoreceptor outer segments [4]. Hyperautofluorescent lipofuscin content is seen in FAF. Furthermore, it has been shown that lipofuscin and its component A2E may have harmful effects on typical RPE cellular functions. Recent studies have examined geographic atrophy (GA), with pathological myopia, patchy atrophy, and several monogenic IRDs, including Best disease and Stargardt disease, using FAF [5]. Curiously, in IRDs like Stargardt illness, Best disease, and retinitis pigmentosa, the changes in FAF intensity are considerably easier to distinguish on FAF photos in comparison to color fundus images. This kind of imaging could be beneficial for IRD follow-up and differential diagnosis in addition to the discovery of afflicted regions [6]. Early/subclinical stages through later stages in IRDs, several phenotypes of FAF changes may be identified in Stargardt illness. FAF may, in particular, Identify the hyperautofluorescent, tiny lesions that resemble the classic Stargardt sickness specks in the high-concentration cytoplasmic A2E. Furthermore, the loss of

1Professor, Department of Computer Science and IT, Jain(Deemed-to-be University), Bangalore-27, India, Email Id: k.suneetha@jainuniversity.ac.in

2Assistant Professor, College of Computing Science and Information Technology, Teerthanker Mahaveer University, Moradabad, Uttar Pradesh, India, Email id: rohailanaaz2@gmail.com

3Assistant professor, School of Computer Science & System, JAIPUR NAITONAL UNIVERSITY, JAIPUR, India, Email Id: shish.dubey@jnujaipur.ac.in

4Assistant Professor, School of Engineering and Computer, Dev Bhoomi Uttarakhand University, Uttarakhand, India, Email Id: socse.govind@dbuu.ac.in

both RPE and choriocapillaris would make atrophy, which appears in the advanced stages of Stargardt disease, look hypoautofluorescent. The hyperautofluorescent Robson-Holder parafoveal ring is by far typical FAF phenotype in retinitis pigmentosa [7]. Curiously, color fundus photography does not show the Robson-Holder ring. FAF imaging shows multiple phases of the course of Best disease, from enhanced auto fluorescence to atrophy of the photoreceptors, which then results in a reduction in the hyperautofluorescence, and eventually cause the RPE harm [8].

2. Related Works

The study [9] examined multilayer deep convolutional neural network (CNN) was trained to distinguish between FAF pictures from each kind of IRD and normal FAF using FAF photos from individuals with retinitis pigmentosa (RP), Best disease (BD), and Stargardt disease (STGD), as well as a healthy similar group. With the help of 389 FAF images, the CNN was trained and verified. The study [10] intended to build an electronic diagnosis method to help ophthalmologists screen in order to prevent diabetic macular edema and stroke by locating the first DR indications during retinal fundus pictures. This study's major goal is to identify and categorize DR according to employing a reworked grey-wolf optimizer changeable built-up weight of a hybrid deep-learning convolutional neural network, or DLCNN-MGWO-VW. The paper [11] mentioned that segment the diabetes-related non-proliferative diabetic retinopathy (NPDR) lesion. With prompt NPDR illness identification, the chance of vision loss can be reduced by 95%. The suggested effort intended to segment the "hard exudate" NPDR lesion. The study [12] examined novel component separation and an improved SVM classifier is used in an automated

approach. Sum of minimum (SOM) local difference pattern (LDP) (SOMLDP), which was created based on the calculation of pixel difference, is the suggested feature extraction method. The work [13] suggested a brand-new machine learning-based computer-aided diagnostic (CAD) method that uses evolutionary principles to categorize WD therapy response. Our CAD system's primary architecture is based on the integration of the artificial immune recognition system (AIRS) and improved adaptive particle swarm optimization (IAPSO) algorithms. The study [14] reported will give a thorough description of CNN and RNN applications for analyzing images in medicine. The overall objective is to motivate professionals in medical image interpretation to employ CNNs widely in their investigation and diagnosis. This chapter highlights the chance of a lifetime opportunity to predict and manage Alzheimer's disease through the evolution of numerous unique DL-based methodologies and models, as well as improvements while using rapid computation methods. The article [15] presented raises crucial queries about the diagnosis of cardiovascular disease (CVD) utilizing this potent but incompletely understood technology. It examines problems caused because of the paradigm change between AI and DL in CVD diagnosis, offers feasible fixes, and looks ahead to uses of connected machine intelligence in the future.

3. Methodology

We introduced the chaotic vortex search optimized naive bayes (CVSONB) approach in this research, which uses the FAF image data set, Z-score normalization as a following step, and Gaber filter bank (GFB) as a second step for feature extraction. Finaly the proposed methodlogy is used for classification of inherited retinal conditions.
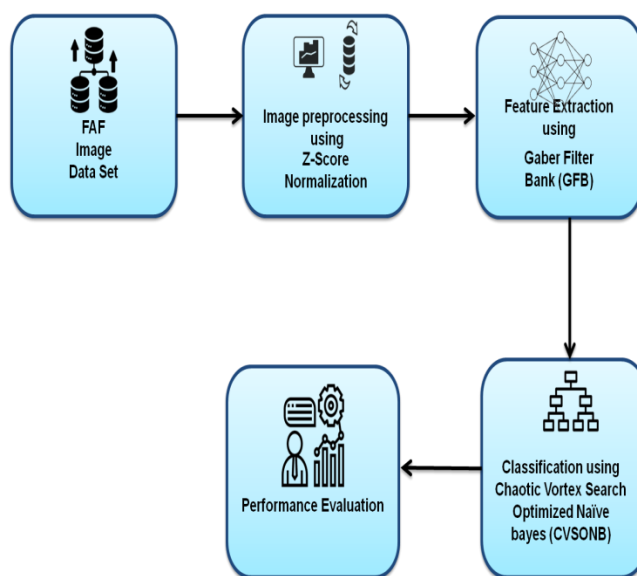

Fig.1. Flow of proposed methodlogy

3.1 Dataset FAF Image

The principles of the Declaration of Helsinki were followed in conducting this retrospective investigation. This investigation received the Federation France Macula 2018-27 Ethics Committee's blessing and was conducted in accordance with French law. Due to the study's retrospective character, written permission was waived. Retinitis pigmentosa (RP), Best diseases (BD), and Stargardt disease (STGD) are three of the most common IRDs. This retrospective investigation comprised the Department of Ophthalmology's clients' FAF scanning at the University Paris EST Creteil who presented between April 2007 and April 2019. Two retina experts (A.M. and K.B.) confirmed the STGD, BD, and RP diagnoses for the included eyes using clinical information, the method of inheritance, multimodal imaging, and electroretinogram (ERG) results, and when accessible, genetic testing using molecules. Healthy controls were those patients without any signs of a retinal condition, as evaluated by a retina expert. Images of the retina with the macula in its center were obtained from the Department of Ophthalmology in Créteil, France. At the Department of Ophthalmology's outpatient clinic in Créteil, FAF images had been taken using Spectralis HRA + OCT between April 2007 and the beginning of 2019 (Heidelberg Eye Explorer, Version 1.10.4.0, Heidelberg Engineering, Heidelberg, Germany). Images with a maximum average of 30 frames and 1536 1536 pixel high quality, 30×30 and 55 × 55 degree fields of foveal-focused perspective were taken. All photos have been deidentified, and all identifying information has been removed. The fovea was positioned in the middle and the FAF pictures were resized to 768 by 768 pixels. Two retina experts (A.M. and K.B.) assigned the images the following classifications: normal, STGD, BD, or RP. The normal, STGD, BD, and RP categorization systems were put into place. The photos separated into three groups: the test set (20%), the set of validation (10%), and the practice set (70 percent of the photos). The distribution of the photos a number of training, validation, and testing sets that included done at random. Images were carefully divided away at eye level between the training data to avoid intra-eye interactions, validation data, and test data. Images that were utilized to train tests using the deep learning classifier were conducted.

3.2 Preprocessing using Z-score Normalization

The adjusted value for the property to determine the z-score normalization utilizing the equation below (Han & Kamber, 2006).

$$y = \frac{u - \mu_B}{\sigma_B} \qquad (1)$$

Here, μ_B and σ are the attribute's mean and standard deviation, A. The raw and adjusted feature values are shown by u and y respectively. After normalizing, all feature values are modified to where the mean and standard deviation are 0 and 1, respectively.

3.3 Gaber Filter Bank (GFB) using feature extraction

Gabor filters are highly regarded for their ability to describe texture. The Gabor filters produce combined localization in the transform (spatial-frequency) and original (space) domains. Because is the Gabor functions that modeled after the visual system in humans, they are very capable of interpreting textures. To get localization characteristics of the realms of space and frequency, a filter bank made up of Gabor filters with various dimensions and orientations utilized. A Gabor feature cube is produced as a consequence of convolution of these filters with the supplied picture. A sinusoidal process that is influenced by an envelope that has a Gaussian shape makes up a Gabor filter. A Gabor filter's impulse response is described by

$$g(w, z) = h(w, z)\exp\left(-i2\pi(Vw + Uz)\right) \qquad (2)$$

Where is the imaginary unit, $i.e i = \sqrt{-1}$, $g(w, z)$ his centered at frequency (V, U) and $h(w, z)$ is the Gaussian envelope:

$$h(w, z) = \frac{1}{2\pi\sigma^2}\exp\left(-\frac{w^2 + z^2}{2\sigma^2}\right) \qquad (3)$$

A bank of Gabor filters with M_t scales and M_c directions are used on the specified image. The result as a Gabor feature cube $M_t \times M_c$ feature maps.

3.4 Classification using Chaotic Vortex Search Optimized Naive Bayes (CVSONB)

3.4.1 Naive Bayes

Naive Bayes is a statistical classification technique that makes use of the Thomas Bayes-authored Bayes theorem. Among various classifiers, such Support Vector Machine and decision trees, it is a well-liked one. Despite being straightforward, it outperforms other classifiers. Each record in a dataset T, which has related n-dimensional properties, can be represented $R = (q_1, q_2 \ldots q_n)$ consist of a set of records with n-dimensional attributes, $E_1, E_2, \ldots E_3$ If there p classes $L_1, L_2, \ldots L_o$ given a set of records R. The classifier can predict that the record q_j belongs to class l_j when:

$$O(L_j \setminus Q) > O(L_j \setminus Q) \text{ for } 1 \leq i \leq o, i \neq j.$$
$$\qquad (1)$$

When $O(L_j \setminus Q)$ is maximized, the maximum posterior probability for a set of records is thereby given as:

$$O(L_j \setminus Q) = \frac{O(Q \setminus L_j) O(L_j)}{O(Q)}$$

$$(2)$$

If $O(Q \setminus L_j)$ is maximized, the evaluation of $O(Q \setminus L_j)$ for a dataset with high dimension is difficult, thus the naïve assumption of attribute independent is made thus

$$O(Q \setminus L_j) = \prod_{r=1}^{m} O(Q_r \setminus L_j) = O(Q_1 \setminus L_j) \times O(Q_2 \setminus L_1) \times \dots \times O(Q_m \setminus L_j)$$

$$(3)$$

The classifier of Naïve Bayes can be represented as

$$M_a = \text{argmax } O(L_j) \prod_{r=1}^{m} O(q_r \setminus L_j), l_j \in L$$

$$(4)$$

The most likely class value is described below. Assigning the test record to the class with the highest likelihood is the Bayesian approach.

3.4.2 Chaotic Vortex search optimized algorithm

The vertical flow of the stirred fluids induces a shift in the CVSOA's metaheuristic optimization algorithm, which enters the stimulated mode. Similar to other single-solution algorithms, its procedures are made up of streamlined generation steps. The use of parameters that entirely from the current one answer modifies the generation of CVSOA populations to any generation. Additionally, rendering single-solution depends on how well each review and look for an iteration pass performs in the seek area. This steadiness is attained inside the proposed CVSOA by employing a spiral-shaped pattern of search. There are some layers circles replicate the vortex sampling techniques. The information about CVSOA methods may be briefly defined in the following four steps:

3.4.2.1 Generating the initial solution

Initials of the preparatory procedure 'center' μ0 and 'radius'. the beginning center of the phase (μ0) Equation 5 allows for the computation.

$$\mu_0 = \frac{\text{upperlimit} + \text{lowerlimit}}{2}$$

$$(5)$$

where the bound restrictions for the problem are upperlimit and lowerlimit, which has a vector of definition $c \times 1$ dimensional-space. Then again, σ_0 the starting radius q_0 produced by equation 6.

$$\sigma_0 = \frac{\text{upperlimit} - \text{lowerlimit}}{2} \qquad (6)$$

3.4.2.2 Generating the candidate solutions

To increase the effectiveness of population expansion, potential solutions are developed. $D_s(T)$ In any iterations, where $D_s(T) = \{t_1, t_2, \dots, t_n\}$ $n = 1, 2, 3, \dots, m$ exemplifies

the resolution and m is the total number of potential solutions. Equation 6 illustrates the equation for the multivariate Gaussian distribution.

$$o(w|\mu, \Sigma) = \frac{1}{\sqrt{(2\pi)^c |\Sigma|}} \exp\left\{ -\frac{1}{2}(w - \mu)^S \Sigma^{-1}(w - \mu) \right\}$$

$$(7)$$

In Eq. (8) d represents the size, even though w is the $c \times c$ unpredictable variable's vector, μ indicates the $c \times c$ sampling mean vector (i.e., center), and Σ represents iterative correlation matrix. Equation (9) it appears from the data if the diagonal components (i.e., variances) of the Σ values are equal and the off-diagonal components (covariance, for example) equal 0 (uncorrelated), the distribution's final form will have a sphere. Thus, the value of Σ is calculated using equal variances and equation 8 with zero covariance.

$$\Sigma = \sigma^2[J]_{c \times c}$$

$$(8)$$

Where the equation(8) is represented , σ^2 how variable the distribution is, I speak for the $c \times c$ individuality matrix and σ_0 is the initial radius (q_0) as can see in Eq. (9).

3.4.2.3 Replacement of the current solution

To facilitate the choosing process, the current method is replaced. A remedy (which is the ideal one) $t \in D_0(T)$ is chosen from and retained in memory $D_0(t)$ in order to replace the existing circle center (μ_0). It is necessary to confirm that the potential solutions fit within the search spaces of equation 9 prior to the selection. process. $t_1^j =$

$$\begin{cases} \text{rand.}(\text{upperlimit}^j - \text{lowerlimit}^j) + \text{lowerlimit}^j, t_1^j < \text{lowerlimit}^j \\ \text{lowerlimit}^j \leq t_1^j \leq \text{upperlimit}^j \\ \text{rand.}(\text{upperlimit}^j - \text{lowerlimit}^j) + \text{lowerlimit}, t_1^j > \text{upperlimit}^j \end{cases}$$

$$(9)$$

Where l= 1, 2, …, m and i = 1, 2, …, c, and the term "random" refers to a number that is dispersed randomly. To choose the following solutions, CVSA decreases the vortex size using Eq. (6) and utilizes tas a new center. Consequently, the fresh set of solutions $D_1(t)$ can be produced. If the selected option performs better, It is memorized and takes the place of the best choice.

3.4.2.4 The radius decrement process

In the VSOA, the radius value is reduced on every subsequent pass by using the inverse incomplete gamma function. Probability theory frequently calls for the incomplete gamma function presented in, particularly in situations involving the chi-square distribution equation 10.

$$\gamma(w, b) = \int_0^w f^{-s} s^{b-1} csb > 0$$

$$(10)$$

where b>0 while being the shape variable $w \geq 0$ is a chance factor. comparable to the gamma function's incompleteness, it complements $\Gamma(w, b)$ is typically introduced (Eq. (7)). In Eq. (7), $\Gamma(b)$ is b (1) equation 10.

$$\Gamma(w, b) = \int_0^\infty f^{-s} s^{b-1} csb > 0$$

$$(11)$$

This section will discuss the hybrid version of CVSA and CMs. The center and radius are two crucial components of the CVSA's straightforward design. The center is a position that is currently in effect from which the CVSA can be assessed.

4. Result

We suggested Chaotic Vortex Search Optimized Naive Bayes (CVSONB) in this paper. Accuracy, sensitivity, F1 score and specificity are the usual evaluation criteria. Additionally, we contrasted our recommended approach CVSONB with other popular techniques like SVM, RF, and CNN.

4.1 Accuracy

The degree to which a projected value or categorization matches the actual value or "ground truth" is known as accuracy. It is frequently used to assess the effectiveness of a model or algorithm in the contexts of machine learning and statistics. When calculating accuracy, one divides all of the forecasts made by the number of reliable forecasts. The accuracy of the suggested strategy is contrasted with that of the conventional methods in Figure 2 and Table 1. Figure 2 shows that the proposed method's accuracy is higher when compared to conventional methods.
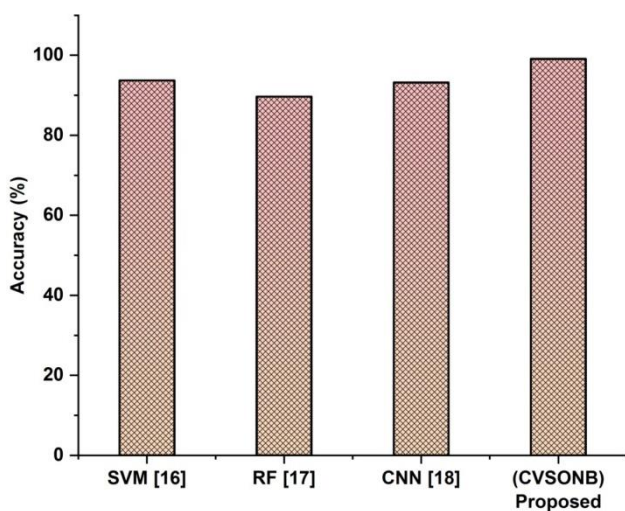

Fig.2 Comparison of Accuracy

Table 1: Computation of Accuracy

Methods	Accuracy (%)
SVM [16]	93.72
RF [17]	89.69
CNN [18]	93.19
(CVSONB) Proposed	99.1

4.2 Sensitivity

Sensitivity is a term used frequently in biology and medicine to describe a test's or a diagnostic tool's capacity to reliably identify positive instances or diseases. It gauges the percentage of true positives that the test successfully found. Sensitivity and specificity are frequently used together to assess how well medical tests function in situations like cancer screenings or illness identification. In Figure 3 and Table 2, the sensitivity of the suggested approach is contrasted with that of the established ones. Figure 3 shows that the proposed method's sensitivity is higher when compared to conventional methods.
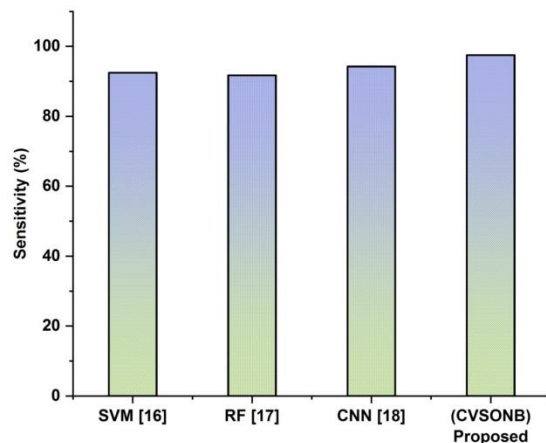

Fig.3 Comparison of Sensitivity

Table: 2 Computation of Sensitivity

Methods	Sensitivity (%)
SVM [16]	92.5
RF [17]	91.74
CNN [18]	94.26
(CVSONB) Proposed	97.52

4.3 F1 score

A popular statistic for assessing a binary detection model's efficacy is the F1 score. It combines precision and recall into a single value that represents the model's overall accuracy. In Figure 4 and Table 3, the F1score of the suggested approach is contrasted with that of the established ones. Figure 3 shows that the proposed method's F1 score is higher when compared to conventional methods.
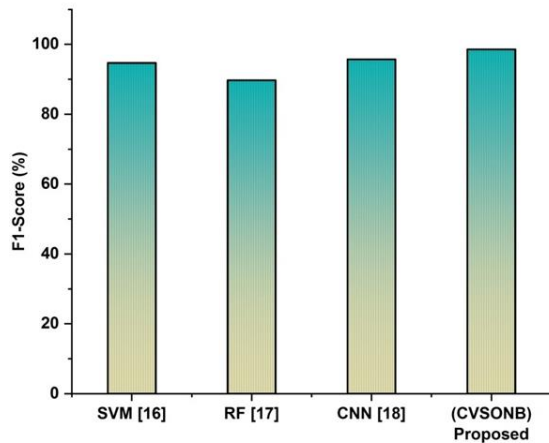

Fig.4 Comparison of F1 score

Table: 3 Computation of F1 score

Methods	F1-Score (%)
SVM [16]	94.7
RF [17]	89.76
CNN [18]	95.72
(CVSONB) Proposed	98.59

4.4 Specificity

specificity, which assesses how well a test can identify people who have a certain ailment, is frequently used in conjunction with specificity. Sensitivity and specificity work together to evaluate a diagnostic test's overall accuracy and dependability. In Figure 5 and Table 4, the specificity of the suggested approach is contrasted with that of the established ones. Figure 5 shows that the proposed method's specificity is higher when compared to conventional methods.
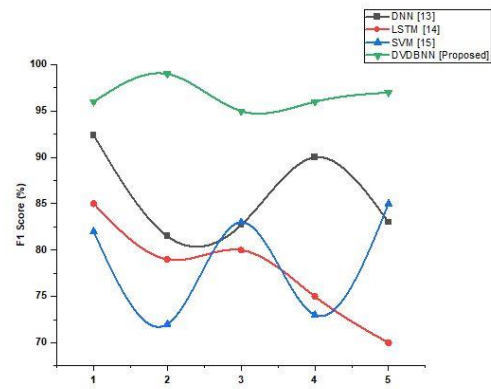

Fig.5 Comparison of Specificity

Table: 4 Computation of Specificity

Methods	Specificity (%)
SVM [16]	95.79
RF [17]	85.25
CNN [18]	96.02
(CVSONB) Proposed	99.7

5. Conclusion

The automated detection and classification of hereditary retinal illness in FAF is described in this article using a deep learning-based method. The Classification of Chaotic Vortex Search Optimized Naive Bayes (CVSONB) so produced great results. This model might become a diagnostic tool and provide useful data for upcoming therapy strategies with further improvement. Additional illness stage classifications were not achievable due to our little sample. However, as IRDs are orphan illnesses, only multi-institutional cooperation would make big datasets accessible. This model might become a diagnostic tool and provide useful data for upcoming therapy strategies with further improvement.

References

[1] Schneider, N., Sundaresan, Y., Gopalakrishnan, P., Beryozkin, A., Hanany, M., Levanon, E.Y., Banin, E., Ben-Aroya, S. and Sharon, D., 2022. Inherited retinal diseases: Linking genes, disease-causing variants, and relevant therapeutic modalities. Progress in Retinal and Eye Research, 89, p.101029.

[2] Schmitz-Valckenberg, S., Pfau, M., Fleckenstein, M., Staurenghi, G., Sparrow, J.R., Bindewald-Wittich, A.,

Spaide, R.F., Wolf, S., Sadda, S.R. and Holz, F.G., 2021. Fundus autofluorescence imaging. Progress in retinal and eye research, 81, p.100893.

[3] Georgiou, Michalis, Kaoru Fujinami, and Michel Michaelides. "Retinal imaging in inherited retinal diseases." Annals of eye science 5 (2020).

[4] Ma, X., Chen, H., Jian, S., He, J., Liu, Y., Han, S., Chang, L., Li, P., Chen, Y.A., Liu, X. and Hu, X., 2023. DAPL1 deficiency in mice impairs antioxidant defenses in the RPE and leads to retinal degeneration with AMD-like features. Redox Biology, 62, p.102675.

[5] Fleckenstein, M., Mitchell, P., Freund, K.B., Sadda, S., Holz, F.G., Brittain, C., Henry, E.C. and Ferrara, D., 2018. The progression of geographic atrophy secondary to age-related macular degeneration. Ophthalmology, 125(3), pp.369-390.

[6] Kumar, D. ., & Sonia, S. (2023). Resources Efficient Dynamic Clustering Algorithm for Flying Ad-Hoc Network. International Journal on Recent and Innovation Trends in Computing and Communication, 11(2s), 106–117. https://doi.org/10.17762/ijritcc.v11i2s.6034

[7] Vázquez-Domínguez, I., Garanto, A. and Collin, R.W., 2019. Molecular therapies for inherited retinal diseases—current standing, opportunities and challenges. Genes, 10(9), p.654.

[8] Marques, J.P., Porto, F.B.O., Carvalho, A.L., Neves, E., Chen, R., Sampaio, S.A.M., Murta, J., Saraiva, J. and Silva, R., 2021. EYS-associated sector retinitis pigmentosa. Graefe's Archive for Clinical and Experimental Ophthalmology, pp.1-9.

[9] Yang, S., Zhou, J. and Li, D., 2021. Functions and diseases of the retinal pigment epithelium. Frontiers in pharmacology, 12, p.727870.

[10] Ghoniem, R.M., 2020. A novel bio-inspired deep learning approach for liver cancer diagnosis. Information, 11(2), p.80.

[11] Reddy, V.P.C. and Gurrala, K.K., 2022. Joint DR-DME classification using deep learning-CNN based modified grey-wolf optimizer with variable weights. Biomedical Signal Processing and Control, 73, p.103439.

[12] Bhandari, S., Pathak, S. and Jain, S.A., 2023. A literature review of early-stage diabetic retinopathy detection using deep learning and evolutionary computing techniques. Archives of Computational Methods in Engineering, 30(2), pp.799-810.

[13] Durai, B. and Raja, J.B., 2023. A bio-inspired fall webworm optimization algorithm for feature selection and support vector machine optimization for retinal abnormalities detection. Multimedia Tools and Applications, pp.1-20.

[14] Abdar, M., Wijayaningrum, V.N., Hussain, S., Alizadehsani, R., Plawiak, P., Acharya, U.R. and Makarenkov, V., 2019. IAPSO-AIRS: A novel improved machine learning-based system for wart disease treatment. Journal of medical systems, 43, pp.1-23.

[15] Bharadwaja, S. and Sasi, S., 2022. Diagnostic Categorization and Neurocognitive Prediction Employing Neuroimaging Data Using Deep Learning in Alzheimer's Illness. In Bio-Inspired Algorithms and Devices for Treatment of Cognitive Diseases Using Future Technologies (pp. 202-223). IGI Global.

[16] Kshirsagar, P. R., Yadav, R. K., Patil, N. N., & Makarand L, M. (2022). Intrusion Detection System Attack Detection and Classification Model with Feed-Forward LSTM Gate in Conventional Dataset. Machine Learning Applications in Engineering Education and Management, 2(1), 20–29. Retrieved from http://yashikajournals.com/index.php/mlaeem/article/view/21

[17] Wong, K.K., Fortino, G. and Abbott, D., 2020. Deep learning-based cardiovascular image diagnosis: a promising challenge. Future Generation Computer Systems, 110, pp.802-811.

[18] Kandhasamy, J.P., Balamurali, S., Kadry, S. and Ramasamy, L.K., 2020. Diagnosis of diabetic retinopathy using multi level set segmentation algorithm with feature extraction using SVM with selective features. Multimedia Tools and Applications, 79, pp.10581-10596.

[19] Chowdhury, A.R., Chatterjee, T. and Banerjee, S., 2019. A random forest classifier-based approach in the detection of abnormalities in the retina. Medical & biological engineering & computing, 57, pp.193-203.

[20] Das, S. and Saha, S.K., 2022. Diabetic retinopathy detection and classification using CNN tuned by genetic algorithm. Multimedia Tools and Applications, 81(6), pp.8007-8020.